Journal of Alzheimer's Disease 91 (2023) 1557–1572
DOI 10.3233/JAD-221152
IOS Press

EEG Entropy in REM Sleep as a Physiologic Biomarker in Early Clinical Stages of Alzheimer's Disease

Hamed Azami[a], Sebastian Moguilner[a], Hector Penagos[b], Rani A. Sarkis[c], Steven E. Arnold[a], Stephen N. Gomperts[a,1,*] and Alice D. Lam[a,1]
[a]*Massachusetts Alzheimer's Disease Research Center, Department of Neurology, Massachusetts General Hospital, Charlestown, MA, USA*
[b]*Picower Institute for Learning and Memory, Massachusetts Institute of Technology, Cambridge, MA, USA*
[c]*Department of Neurology, Brigham and Women's Hospital, Boston, MA, USA*

Accepted 17 December 2022
Pre-press 12 January 2023

Abstract.
Background: Alzheimer's disease (AD) is associated with EEG changes across the sleep-wake cycle. As the brain is a non-linear system, non-linear EEG features across behavioral states may provide an informative physiologic biomarker of AD. Multiscale fluctuation dispersion entropy (MFDE) provides a sensitive non-linear measure of EEG information content across a range of biologically relevant time-scales.
Objective: To evaluate MFDE in awake and sleep EEGs as a potential biomarker for AD.
Methods: We analyzed overnight scalp EEGs from 35 cognitively normal healthy controls, 23 participants with mild cognitive impairment (MCI), and 19 participants with mild dementia due to AD. We examined measures of entropy in wake and sleep states, including a slow-to-fast-activity ratio of entropy (SFAR-entropy). We compared SFAR-entropy to linear EEG measures including a slow-to-fast-activity ratio of power spectral density (SFAR-PSD) and relative alpha power, as well as to cognitive function.
Results: SFAR-entropy differentiated dementia from MCI and controls. This effect was greatest in REM sleep, a state associated with high cholinergic activity. Differentiation was evident in the whole brain EEG and was most prominent in temporal and occipital regions. Five minutes of REM sleep was sufficient to distinguish dementia from MCI and controls. Higher SFAR-entropy during REM sleep was associated with worse performance on the Montreal Cognitive Assessment. Classifiers based on REM sleep SFAR-entropy distinguished dementia from MCI and controls with high accuracy, and outperformed classifiers based on SFAR-PSD and relative alpha power.
Conclusion: SFAR-entropy measured in REM sleep robustly discriminates dementia in AD from MCI and healthy controls.

Keywords: Alzheimer's disease, EEG, entropy, mild cognitive impairment, REM sleep, sleep

INTRODUCTION

A growing number of biomarkers have been developed to assist in the diagnosis and staging of Alzheimer's disease (AD), the most common neurodegenerative disease and dementia [1–3]. Amyloid and tau assessments via positron emission tomography (PET) imaging, cerebrospinal fluid

[1]Dr. Stephen Gomperts and Dr. Alice Lam contributed equally to this work.

*Correspondence to: Stephen N. Gomperts, MD, PhD, 114 16th Street, Room 2004, Massachusetts Alzheimer's Disease Research Center, MassGeneral Institute for Neurodegenerative Disease, Department of Neurology, Massachusetts General Hospital, Charlestown, MA, USA. Tel.: +1 617 726 5570; E-mail: gomperts.stephen@mgh.harvard.edu.

(CSF) analysis, and recently developed blood-based measurements complement multiple measures of neurodegeneration, including structural magnetic resonance imaging (MRI) measures of atrophy, CSF and blood analytes, and functional measures such as fluorodeoxyglucose PET, functional MRI, and electroencephalography (EEG) [4–7]. Together, these biomarkers provide a broad characterization of the disease process.

From its earliest stages, AD is characterized by synaptic dysfunction and circuit failure [6, 8]. Scalp EEG offers high temporal resolution measurements of the brain's electrical activity and is both non-invasive and cost-effective [7, 9, 10]. As such, scalp EEG may be a promising tool to assess the neurophysiologic changes that arise in AD.

Analysis of brief periods of awake resting-state EEG (rsEEG) has been explored extensively for the development of EEG biomarkers for AD and mild cognitive impairment (MCI) [11, 12]. Power spectrum and functional connectivity-based methods have been widely employed to characterize rsEEGs in MCI and AD [7, 11, 13]. Most such analyses have been based on relative power spectral density (rPSD) of the rsEEG and have demonstrated increases in spectral power at lower frequency bands (theta and delta) in individuals with AD, and to a lesser extent, those with MCI, compared to age-matched healthy controls [11, 12, 14]. Yet, despite a large number of studies in this area, the diagnostic accuracy of rsEEG in AD remains controversial, and there is currently insufficient evidence to recommend rsEEG as part of the diagnostic workup for AD [11, 15, 16].

Although the earliest stages of AD are associated with sleep disturbances, and a growing literature has demonstrated important changes in sleep neurophysiology over the course of AD, including changes in sleep macro-architecture (increased sleep fragmentation and reduced time in deeper stages of sleep) [17, 18], analysis of sleep EEG in AD has received relatively little attention to date. Even so, in non-rapid eye movement (NREM) sleep, a number of reports have described AD-associated changes in sleep spindles, K-complexes, slow wave activity, and spindle-slow wave coupling, some of which correlate with the burden of amyloid and/or tau pathology, or with changes in cognitive function [19–25].

As rapid eye movement (REM) sleep engages basal forebrain cholinergic neurons, which degenerate early and prominently in AD [26–28] and which are differentially active across sleep and waking states [29–31], there is reason to anticipate that changes in REM sleep would also be a feature of early AD. Indeed, a limited series of studies 30 years ago evaluating EEG spectral changes in AD found that spectral changes during REM sleep more accurately distinguished AD from healthy controls than spectral changes during the awake state [32]. In particular, the ratio of power in the slow frequencies (delta and theta) over that in the fast frequencies (alpha and beta), referred to here as the slow-to-fast activity ratio of the power spectral density (SFAR-PSD), was found to be significantly greater during REM sleep in individuals with mild to moderate AD dementia, compared to healthy controls [32]. Whether this intriguing finding is in fact robust has been unclear.

Cognition and higher-order perception, which deteriorate in MCI and AD, originate from the collective activity of a large number of neurons within cortical circuits and across the brain's large-scale systems [7, 33]. Modeling large-scale brain activity with nonlinear dynamical approaches based on information theory, such as entropy, allows the integration of experimental data from multiple modalities into a collective framework. It has been demonstrated that collective, nonlinear dynamics are fundamental to adaptive cortical activity and linked to a number of brain disorders [7, 34, 35]. To this end, entropy approaches have been used to detect nonlinear dynamics of the EEG. However, existing entropy approaches have been used to quantify the irregularity of signals at one temporal scale and may fail to account for the multiple time-scales inherent in electrophysiological recordings [36, 37]. To detect EEG dynamics across a range of biologically relevant time-scales that span from delta to gamma oscillations, multiscale non-linear methods such as multiscale fluctuation dispersion entropy (MFDE) are of particular interest, as they are sensitive to fluctuation changes in EEG time series over these time scales [37].

To date, the examination of MFDE in AD has primarily been performed on awake rsEEG [38]. We hypothesized that its application across sleep states would be of particular value in discriminating AD, where impairments of the sleep EEG and cholinergic cell loss are prominent. Thus, we evaluated MFDE of sleep EEG in participants with mild dementia and MCI due to probable AD, as well as healthy cognitively normal older adults, and compared MFDE to rPSD and relative alpha power across sleep states.

MATERIALS AND METHODS

Standard protocol approvals, registrations, and patient consents

All study procedures were performed under a protocol approved by the Institutional Review Board at our Center. Written informed consent was obtained from all prospectively recruited research participants.

Study population

Ambulatory EEG recordings analyzed in this study were acquired both prospectively and retrospectively. Some EEGs were collected prospectively from research participants, and others were obtained retrospectively from patients who underwent ambulatory EEG for clinical purposes, as previously described [39]. A subset of EEGs analyzed in this study came from participants from the prior study who met our inclusion and exclusion criteria below and whose EEGs had undergone manual sleep scoring as part of another study [40]. To improve diagnostic purity of our sample in this study, we excluded all individuals who had a history of epilepsy.

Inclusion criteria for this study were: 1) Age 60–85 years at time of EEG; and 2) Clinical classification into one of 3 groups: cognitively normal healthy controls (HC); MCI due to probable AD (MCI), determined according to the National Institute of Aging-Alzheimer's Association criteria [41]; and mild dementia due to probable AD (DEM), determined according to the National Institute of Aging-Alzheimer's Association criteria [42]. All HC had neurocognitive test scores within the normal range and Clinical Dementia Rating global score of 0. MCI and DEM had Clinical Dementia Rating global scores of 0.5 and 1, respectively, at the time of EEG. Exclusion criteria for this study were: 1) history of epilepsy, stroke, traumatic brain injury with loss of consciousness, meningitis/encephalitis, brain tumor, or brain surgery; and 2) current use of benzodiazepines, sleep aids, or bupropion. No participants had clinical or biomarker features to support a diagnosis of MCI with Lewy bodies or dementia with Lewy bodies (parkinsonism, REM sleep behavioral disorder, hallucinations or indicative biomarkers), an alternative parkinsonian dementia, frontotemporal dementia, or vascular dementia [43–45]. Two cognitive neurologists (SG, AL) reviewed all MCI and DEM cases to adjudicate diagnoses based on the above criteria; their consensus diagnosis was used for group classifications.

Cognitive testing

Montreal Cognitive Assessment (MoCA) and Mini-Mental State Exam (MMSE) scores were obtained either from clinical workup or as part of research study procedures. We analyzed scores that were performed within 1 year of the EEG (mean $\pm$ std: 101 ± 98 days). If participants had multiple test scores within 1 year of the EEG, we selected the one closest in time to the EEG study. MMSE scores were converted to the equivalent MoCA score, based on the conversion table from [46].

EEG acquisition, sleep scoring, and pre-processing

Ambulatory EEG enables long-term monitoring of brain activity in realistic, dynamic environments. This technique, compared with routine EEG and long-term monitoring in a hospital, benefits from low cost, convenience, and the ability to capture circadian patterns. Acquisition of ambulatory EEG recordings in the study was as described previously [39]. In short, scalp EEG electrodes were placed according to the International 10–20 system with additional anterior temporal (T1, T2) electrodes. EEGs were recorded using XLTEK TREX hardware (Natus Medical Inc, Pleasanton, CA) with sampling rate of 200 Hz. Ambulatory EEG recording data used in this study spanned from 10 to 48 h. All ambulatory EEGs were visually reviewed in entirety by two board-certified clinical neurophysiologists (ADL, RAS) to ensure quality of the recordings. EEGs were manually sleep scored by a single sleep technician (blinded to diagnosis), using 5 sleep stages (wake, NREM1, NREM2, NREM3, and REM), according to American Academy of Sleep Medicine (AASM) criteria as described previously [40].

For pre-processing, EEGs were digitally band-pass filtered in both forward and reverse directions to avoid net phase shift, with a Hamming window FIR filter of order 200 and cut-off frequencies at 1 Hz and 40 Hz. EEG data were analyzed with channels in an anterior-posterior longitudinal bipolar montage (Fp1-F7, F7-T3, T3-T5, T5-O1, Fp1-F3, F3-C3, C3-P3, P3-O1, Fz-Cz, Cz-Pz, Fp2-F4, F4-C4, C4-P4, P4-O2, Fp2-F8, F8-T4, T4-T6, T6-O2). We analyzed the data across the whole brain (all channels) as well as in five brain regions, including frontal (Fp1-F7,

Fp1-F3, F3-C3, Fz-Cz, Fp2-F8, Fp2-F4, F4-C4), temporal (F7-T3, T3-T5, T5-O1, F8-T4, T4-T6, T6-O2), central (F3-C3, F4-C4, C3-P3, C4-P4, Fz-Cz, Cz-Pz), parietal (C3-P3, C4-P4, P3-O1, P4-O2, Cz-Pz), and occipital (T5-O1, P3-O1, T6-O2, P4-O2).

Power spectral density analysis

Power spectra were computed from band-passed EEG data based on discrete Fourier transform and normalized to the total power in the spectrum (relative PSD). Each EEG was divided into non-overlapping 30-s epochs, aligned with the manual sleep scoring. Each 30-s epoch was further divided into non-overlapping 3-s windows, and a PSD was calculated for each 3-s window, for each channel. A sleep-stage specific PSD was then determined for each patient, by calculating the median PSDs across all 3-s windows in a given sleep stage (awake, N1, N2, REM), for each channel. Median values were used to minimize the potential effects of outliers related to noise or artifact in the EEG recordings. SFAR-PSD was also calculated as: (delta + theta) / (alpha + beta), using spectral band power in slow and fast frequency ranges, with delta: 0.5–4 Hz, theta: 4–8 Hz, alpha: 8–12 Hz, and beta: 12–32 Hz [47]. Relative alpha power was calculated as the power in the alpha band divided by the total power in the frequency band 1–40 Hz.

Multiscale fluctuation dispersion entropy

MFDE is based on fluctuation dispersion entropy (FDispEn) and provides insight into the complexity of fluctuations over a range of time scales [37, 38]. DispEn and its fluctuation form (FDispEn) are recently proposed entropy metrics based on Shannon entropy and fluctuation dispersion patterns [48, 49]. Dispersion entropy-based methods detect change in amplitude, frequency, bandwidth, noise power, and periodicity of time series [48, 49]. These entropy approaches have been applied in a variety of settings in biomedical signal analysis, including rsEEG and sleep EEG [37, 50, 51], magnetoencephalography [37], cardiac activity [52, 53], and heart sounds [54], among others. As FDispEn is faster than DispEn and needs a lower number of samples for a reliable estimation of entropy [49], we elected to use MFDE in this study. Formally, MFDE is computed as follows [38].

Assume a univariate discrete time series of length L: $\mathbf{u} = \{u_1, u_2, \ldots, u_L\}$. First, the original signal $\mathbf{u}$ is divided into non-overlapping segments of length τ, called temporal scale factor. Next, the average of each segment is calculated to derive the coarse-grained time series as follows:

$$x_j^{(\tau)} = \frac{1}{\tau} \sum_{b=(j-1)\tau+1}^{j\tau} u_b \qquad 1 \le j \le \frac{L}{\tau} = N. \quad (1)$$

Finally, the FDispEn value is calculated for each coarse-grained signal.

The FDispEn of the univariate signal of length N: $\mathbf{x} = \{x_1, x_2, \ldots, x_N\}$ is defined as follows:

1) $x_j\,(j = 1, 2, \ldots, N)$ are first mapped to c classes with integer indices from 1 to c. For this purpose, the normal cumulative distribution function (NCDF) is first used to overcome the problem of assigning most of x_i to only a few classes when maximum or minimum values are considerably larger or smaller than the median/mean value of the time series. The NCDF maps $\mathbf{x}$ into $\mathbf{y} = \{y_1, y_2, \ldots, y_N\}$ between 0 and 1 as follows:

$$y_j = \frac{1}{\sigma\sqrt{2\pi}} \int_{-\infty}^{x_j} e^{\frac{-(t-\mu)^2}{2\sigma^2}}\, \mathrm{d}t \quad (2)$$

where μ and σ are respectively the mean and SD of signal $\mathbf{x}$. Afterwards, we use a linear mapping to assign each y_i to an integer from 1 to c. To this end, for each member of the mapped time series, we use $z_j^c = \text{round}\left(c \cdot y_j + 0.5\right)$, where z_j^c shows the j^{th} member of the classified signal and rounding involves either increasing or decreasing a number to the next digit.

2) $\mathbf{z}_i^{m,c}$ are made with embedding dimension m and time delay d according to $\mathbf{z}_i^{m,c} = \left\{z_i^c, z_{i+d}^c, \ldots, z_{i+(m-1)d}^c\right\}$, $i = 1, 2, \ldots, N - (m-1)\,d$. Each vector $\mathbf{z}_i^{m,c}$ is mapped to a dispersion pattern $\pi_{v_0 v_1 \ldots v_{m-1}}$, where $z_i^c = v_0, \quad z_{i+d}^c = v_1, \ldots, z_{i+(m-1)d}^c = v_{m-1}$. The number of possible fluctuation-based dispersion patterns that can be assigned to each vector $\mathbf{z}_i^{m,c}$ is equal to $(2c-1)^{m-1}$.

3) For each $(2c-1)^{m-1}$ potential dispersion patterns $\pi_{v_0 v_1 \ldots v_{m-1}}$, relative frequency is calculated as follows:

$$p\left(\pi_{v_0 \ldots v_{m-1}}\right) = \frac{\#\left\{i \,\middle|\, i \le N-(m-1)\,d, \mathbf{z}_i^{m,c} \text{ has type } \pi_{v_0 \ldots v_{m-1}}\right\}}{N-(m-1)\,d} \quad (3)$$

where # means cardinality. In fact, $p\left(\pi_{v_0 v_1 \ldots v_{m-1}}\right)$ denotes the number of dispersion patterns of $\pi_{v_0 v_1 \ldots v_{m-1}}$ that is assigned to $\mathbf{z}_i^{m,c}$, divided by the

total number of embedded vectors with embedding dimension m.

4) Finally, according to the definition of Shannon entropy, the FDispEn is defined as follows:

$$FDispEn\,(\mathbf{x}, m, c, d) = -\sum_{\pi=1}^{(2c-1)^{m-1}} p\left(\pi_{v_0 \ldots v_{m-1}}\right) \cdot \ln\left(p\left(\pi_{v_0 \ldots v_{m-1}}\right)\right) \quad (4)$$

Multiscale entropy techniques at scale factor τ can be considered as a low-pass filter with cut-off frequency $\frac{f_s}{2\tau}$ [55]. Based on this fact, MFDE at $\tau = 5$ and $\tau = 20$ correspond to the frequency band 1–20 Hz and 1–5 Hz, respectively. In this study, we investigate the effect of DEM or MCI on entropy in lower relative to higher frequency components.

For MFDE (and all other entropy measures described below), each EEG was divided into non-overlapping 30-s epochs, aligned with the manual sleep scoring. Each 30-s epoch was further divided into non-overlapping 3-s windows, and MFDE was calculated in each 3-s window, for each channel. A sleep-stage specific MFDE was then determined for each patient, by calculating the median MFDE value across all 3-s windows from a given sleep stage (awake, N1, N2, and REM), for each channel. As with PSD, median values were used to minimize the potential effects of outliers related to noise or artifact in the EEG recordings. The SFAR-entropy measure was calculated as: (MFDE at scale 20) / (MFDE at scale 5).

Code for calculating MFDE can be found at: https://github.com/HamedAzami. Topoplots of MFDE values were created in MATLAB using code available at: https://www.mathworks.com/matlabcentral/fileexchange/72729-topographic-eeg-meg-plot. For each diagnostic group, coefficients of variation (ratio of the standard deviation to the mean) of SFAR-entropy and SFAR-PSD within each period of REM sleep were calculated for each individual patient and averaged.

Other entropy measures

Multiscale fuzzy entropy (MFE) is a conditional entropy-based measure that calculates a modification of sample entropy—fuzzy entropy—over multiple time scales [56]. MFE, unlike multiscale sample entropy, does not lead to undefined or unreliable values, especially for short signals [38, 56].

Multiscale dispersion entropy (MDE) is a distinct nonlinear measure quantifying the dynamical variability of the fluctuations of signals over multiple time scales [38]. Code for calculating MFE and MFDE can be found at: https://doi.org/10.7488/ds/1477 and https://doi.org/10.7488/ds/1982, respectively.

Classification models

We trained logistic regression classifiers to distinguish DEM from MCI; DEM from HC; and MCI from HC, using either occipital SFAR-entropy (based on MFDE), SFAR-PSD, or relative alpha power as the input. Additional models that included demographic features of age, sex, and level of education were also explored. Logistic regression was implemented using the Scikit-learn library [57] with default hyperparameters. We used a leave-one-participant-out cross validation where, for each model and a dataset of size n participants, we used *n-1* participants to train the model and tested the model using the 1 left-out participant. This procedure was repeated n times, testing on each participant once. We then determined the overall cross-validation performance of the model across all n left-out participants. We evaluated the cross-validated performance of each model using the area under the Receiver Operating Characteristic curve (AUC_{ROC}) and the area under the Precision-Recall Curve (AUC_{PR}). For each model, 95% confidence intervals were obtained by bootstrapping, using 1000 random sub-samples, each 90% of the total sample size, stratified by diagnostic group, with replacement. The same features were used during training and testing in each model, i.e., no feature elimination approaches were used. Statistical comparisons of model performances were assessed using a non-parametric p-value estimation based on the calculated confidence intervals [58].

Statistical analysis

Group statistical comparisons were performed using analysis of variance (ANOVA) with Tukey *post hoc* pairwise comparisons. Relationships between continuous measures were assessed with Spearman correlations. Group statistics are reported as means $\pm$ standard deviations, unless otherwise stated. Statistical analyses were conducted using MATLAB version 2018a. ANOVA p-values were Bonferroni corrected for multiple comparisons.

RESULTS

Study population demographics

EEG data were analyzed from 35 HC, 23 MCI, and 19 DEM participants. The demographics of our study population are shown in Table 1. Additional biomarker evidence indicating AD pathology (CSF, Pittsburgh compound B PET, or autopsy) was available for 1 MCI and 4 DEM participants. There were no significant differences between groups with respect to age, gender, years of education, or the relative distribution of sleep stages seen in each group, as a percentage of total time in sleep. Acetylcholinesterase inhibitor use was common in MCI and DEM.

Whole brain MFDE across the sleep-wake cycle

We first calculated whole brain-averaged MFDE across a range of entropy scale factors. We assessed group differences in this measure across states of wakefulness and sleep (NREM1, NREM2, and REM) (Fig. 1A). NREM3 sleep was excluded, as most participants (83% of HC, 75% of MCI, and 67% of DEM), had no NREM3 sleep observed during their EEG study. The MFDE curves for HC, MCI, and DEM were qualitatively similar in the awake, NREM, and REM states, with differences in MFDE between groups seen at both low and high entropy scale factors. At low scale factors, the DEM group had lower MFDE values compared to MCI and HC, while at high scale factors, the DEM group had higher MFDE values compared to MCI and HC.

Given that the group differences in MFDE at low and high scale factors occurred in opposite directions, we calculated a slow-to-fast activity ratio of the MFDE (SFAR-entropy), as the ratio of MFDE at a scale factor of 20 (1–5 Hz band) to MFDE at a scale factor of 5 (1–20 Hz band), to see if this would provide facile discrimination between groups (Fig. 1B). The ANOVA *p*-values were corrected based on the Bonferroni method for 4 comparisons.

In REM sleep, the whole-brain averaged SFAR-entropy was significantly higher in DEM than in HC, and also in DEM compared to MCI (corrected ANOVA, $p = 2\text{e-}4$; *post hoc* comparison of DEM versus HC, $p = 2\text{e-}6$; *post hoc* comparison of DEM versus MCI, $p = 0.007$). In contrast, there was reduced discrimination between groups using whole brain-averaged SFAR-entropy in the awake, NREM1, and NREM2 stages. No significant differences were seen between any of the groups in the NREM2 stage. In the awake state, there was a significant difference between DEM versus HC, but not between DEM versus MCI (corrected ANOVA, $p = 0.038$; *post hoc* comparison of DEM versus HC, $p = 0.0083$; *post hoc* comparison of DEM versus MCI, $p > 0.05$). Similarly, in the NREM1 stage, there was a significant difference between DEM versus HC, but not between DEM versus MCI (corrected ANOVA, $p = 0.0032$; *post hoc* comparison of DEM versus HC, $p = 5\text{e-}4$; *post hoc* comparison of DEM versus MCI, $p > 0.05$).

REM sleep is characterized by rapid phasic eye movements, which can contaminate frontal and temporal EEG channels with large amplitude eye movement artifacts. To ensure that our results in REM sleep were not simply related to eye movement artifacts, we repeated the calculations above, while excluding channels from the frontal and temporal regions and found that the results for the REM sleep analysis were unchanged (corrected ANOVA, $p = 8\text{e-}4$; *post hoc* comparison of DEM versus HC, $p = 1\text{e-}4$; *post hoc* comparison of DEM versus MCI, $p = 0.016$; Supplementary Figure 1). Together, these results demonstrate that whole brain-averaged MFDE is significantly different in individuals with DEM compared to both MCI and HC, and that these differences are most prominent in REM sleep.

Brain regional differences in MFDE during REM sleep

We next evaluated whether the differences in SFAR-entropy during REM sleep in DEM were enriched within specific brain regions. Figure 2A shows topoplots of MFDE for each group, calculated at a scale of 5 (top row), a scale of 20 (middle row), and at an MFDE ratio of scales 20 to 5 (SFAR-entropy; bottom row). We also calculated the average SFAR-entropy within specific brain regions, including frontal, temporal, central, parietal, and occipital (Fig. 2B). The ANOVA *p*-values were corrected based on the Bonferroni method for 5 comparisons.

Significant differences between DEM and HC, and between DEM and MCI, were seen for all brain regions assessed (Fig. 2B). Group differences in SFAR-entropy were greatest within the temporal region (corrected ANOVA: $p = 2\text{e-}5$; *post hoc* comparison of DEM versus MCI, $p = 0.002$; *post hoc* comparison of DEM versus HC, $p = 2\text{e-}6$). After the temporal lobe, the lowest ANOVA *p*-value was obtained in the occipital lobe (corrected ANOVA:

Table 1
Study population demographics and sleep macro-architecture

	HC	MCI	DEM	ANOVA p
Participants (n)	35	23	19	–
Age, y (SD)	75.5 (6.9)	75 (6.9)	72.2 (6)	NS
Female (# / %)	20 / 57%	15 / 65%	9 / 47%	NS
Years of Education (SD)	16.9 (2.7)	16.2 (2.3)	15.3 (3.4)	NS
Global CDR score (SD)	0 (0)	0.5 (0)	1 (0)	
Cholinesterase inhibitor use (# / %)	0 / 0%	9 / 39%	13 / 68%	p = 1e-8;
MoCA score (SD)	28 (1.8)	23.3 (3)	13.9 (6.4)	HC versus MCI, p = 0.0004; HC versus DEM p = 1e-8; MCI versus DEM, p = 0.028 p = 2e-15; HC versus MCI, p = 1e-04; HC versus DEM p = 9e-10; MCI versus DEM, p = 3e-9
Sleep Macro-Architecture				
Total sleep, min (SD)	375 (88)	368 (105)	406 (99)	NS
N1 sleep, min (SD)	57 (29)	46 (24)	51 (26)	NS
N2 sleep, min (SD)	227 (72)	216 (73)	264 (92)	NS
N3 sleep, min (SD)	1 (3)	8 (21)	6 (18)	NS
REM sleep, min (SD)	89 (39)	98 (53)	85 (44)	NS
% N1 sleep	15% (7%)	13% (8%)	13% (7%)	NS
% N2 sleep	60% (10%)	59% (12%)	64% (13%)	NS
% N3 sleep	0.2% (0.8%)	2% (6%)	1.4% (4.3%)	NS
% REM sleep	24% (9%)	25% (10%)	21% (9%)	NS

SD, standard deviation.

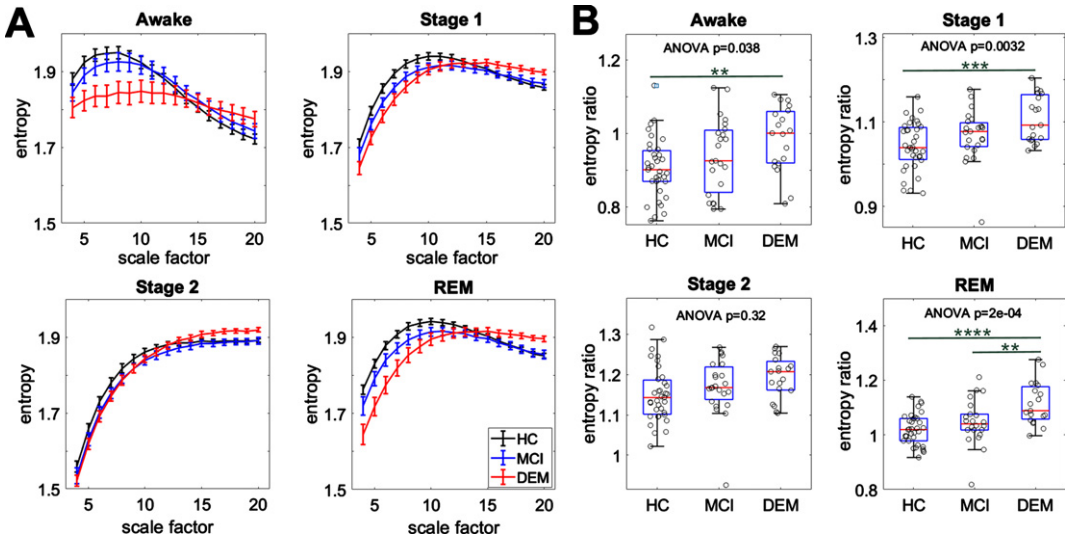

Fig. 1. Assessment of whole-brain averaged MFDE across the sleep-wake cycle in AD. A) Whole brain-averaged multiscale fluctuation dispersion entropy (MFDE) measured from EEG across awake and sleep states in 35 HC (black), 23 MCI (blue), and 19 DEM (red) participants. B) Slow-to-fast activity ratio for MFDE (SFAR-entropy) across awake and sleep states for HC, MCI, and DEM. ANOVA p-values are shown for each boxplot (Bonferroni corrected). Statistically significant *post-hoc* comparisons with p-values<0.01, 0.001, and 0.0001 are shown with **, ***, and ****, respectively.

p = 3e-5; *post hoc* comparison of DEM versus MCI, p = 0.002; *post hoc* comparison of DEM versus HC, p = 6e-6). As such and given that the occipital lobe is the region least affected by eye movement artifacts in REM sleep, we carried out the remainder of our analyses using SFAR-entropy in the occipital region during REM sleep.

Group differences in MFDE are not related to use of acetylcholine esterase inhibitors

To determine whether group differences in SFAR-entropy were impacted by differential use of acetylcholine esterase inhibitors, we repeated the analyses in participants not using acetylcholine

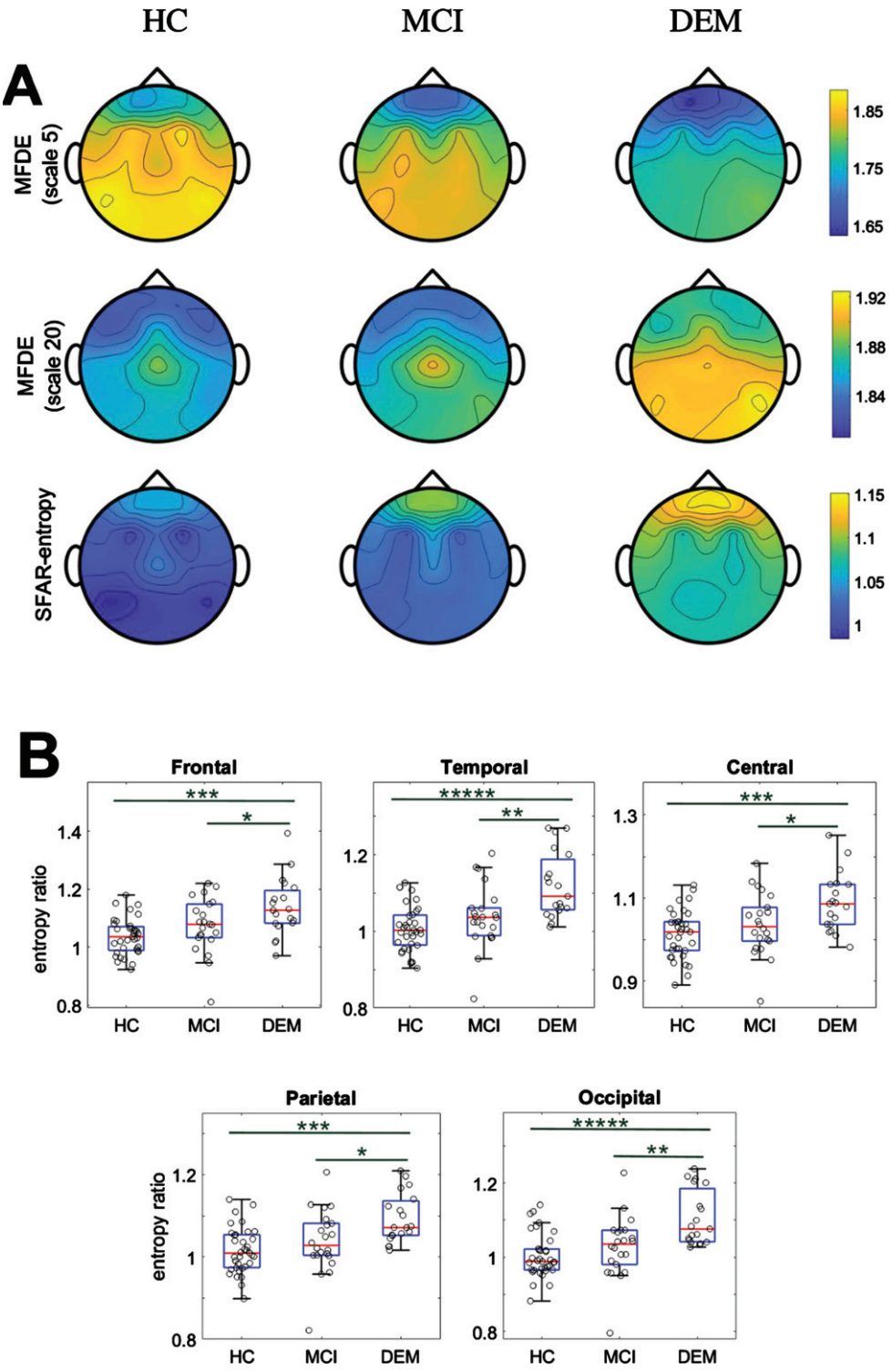

Fig. 2. Evaluation of regional REM sleep-associated MFDE changes in AD. A) Topoplots of averaged MFDE values during REM sleep at scale 5 (top row) and scale 20 (middle row), and the ratio of MFDE at scale 20 to scale 5 (SFAR-entropy, bottom row) for HC, MCI, and DEM. B) SFAR-entropy in the frontal (ANOVA, $p = 1e\text{-}03$), temporal (ANOVA, $p = 2e\text{-}05$), central (ANOVA, $p = 2e\text{-}03$) parietal (ANOVA, $p = 1e\text{-}03$), and occipital (ANOVA, $p = 3e\text{-}05$) regions for HC, MCI, and DEM. ANOVA p-values are Bonferroni corrected. Group differences with p-values<0.05, 0.01, 0.001, 0.0001, and 0.00001 are shown with *, **, ***, ****, and *****, respectively.

esterase inhibitors. In this subset analysis, SFAR entropy in the occipital region during REM sleep continued to differentiate DEM from MCI and HC groups (ANOVA, $p = 0.0046$; *post hoc* comparison of DEM versus HC, $p = 0.0031$, Hedge's g effect size = 1.71; *post hoc* comparison of DEM versus MCI, $p = 0.031$, Hedge's g effect size = 0.96; Supplementary Figure 2). Thus, the group differences in SFAR entropy in REM sleep were not a result of differential acetylcholinesterase inhibitor use.

Group differences in MFDE are stable across REM cycles over the night

To determine whether the SFAR-entropy measure during REM sleep might change with REM sleep cycles over the night, we calculated SFAR-entropy in the occipital region, in the first, middle, and last 5 min of REM sleep (Fig. 3A). The ANOVA *p*-values were corrected based on the Bonferroni method for three comparisons.

SFAR-entropy was stable across REM cycles within diagnostic groups (corrected ANOVA *p*-values<0.001), showing significant differences between DEM and HC (*post-hoc p*-values<0.0001), and between DEM and MCI (*post-hoc p*-values<0.05) in each REM epoch.

We also compared these measures to SFAR-PSD and relative alpha power calculated in the occipital regions in the same REM epochs. SFAR-PSD showed statistically significant differences between DEM and HC in the middle and last 5 min of REM sleep (corrected ANOVA *p*-values<0.01, *post-hoc p*-values<0.01; Fig. 3B). SFAR-PSD also showed significant differences between DEM and MCI, but only in the last REM epoch (*post-hoc p*-value = 0.021). Relative alpha power in the occipital region was stable across REM epochs, with statistically significant differences between DEM and HC across all epochs (ANOVA *p*-values<0.01, *post-hoc p*-values<0.01; Fig. 3C). Relative alpha power significantly differed between HC and MCI in the middle REM epoch alone (*post-hoc p*-value = 0.007).

To further evaluate the stability of the SFAR-entropy, SFAR-PSD, and relative alpha power measures during REM sleep, we examined their coefficients of variation (CV; ratio of the standard deviation to the mean) across REM sleep in HC, MCI, and DEM participants (Table 2). Across all diagnostic groups, the CV for SFAR-entropy was significantly lower than the CV for SFAR-PSD and relative alpha power. Thus, the SFAR-entropy measure showed greater stability during REM sleep than SFAR-PSD and relative alpha power.

Comparison of MFDE to other entropy and spectral measures in REM sleep

We next compared the MFDE-based SFAR-entropy to other entropy measures, namely MFE and MDE, and to spectral measures (SFAR-PSD, relative delta power, and relative alpha power) in REM sleep (Fig. 4). All measures were calculated in the occipital region. While almost all measures showed significant group differences between DEM and MCI, and between DEM and HC, the entropy measures (MFDE, MFE, and MDE) consistently showed the greatest corrected effect sizes for the discrimination of DEM from HC (Hedge's g effect sizes: MFDE, 1.61; MFE, 1.46; MDE, 1.56; SFAR-PSD, 1.25; delta, 1.43; alpha, 1.34). Interestingly, relative alpha power was the only measure that showed a significant difference between MCI versus HC ($p = 0.031$), but this measure did not show a significant difference between DEM versus MCI ($p = 0.17$).

SFAR-entropy in REM sleep is significantly correlated with global cognitive function

As the increases in low frequency EEG activity and reductions in higher frequency EEG activity that we observed in DEM could provide a simple quantitative measure of neural systems failure, we next examined how SFAR-entropy, SFAR-PSD, and relative alpha power in the occipital region during REM sleep related to cognitive function as measured with the MoCA (Fig. 5). MoCA scores were available for 91% of MCI and 63% of DEM, with a mean time between EEG and cognitive testing of 101 ± 98 days. SFAR-entropy, SFAR-PSD, and relative alpha power were all significantly correlated with MoCA score (SFAR-entropy correlation, Spearman $\rho = -0.47$, $p = 0.0001$; SFAR-PSD correlation, Spearman $\rho = -0.47$, $p = 0.0001$; relative alpha power correlation, Spearman $\rho = +0.45$, $p = 0.0003$).

Diagnostic classification based on SFAR-entropy in REM sleep

We trained separate logistic regression models to classify DEM versus HC, DEM versus MCI, and MCI versus HC, using either occipital SFAR-entropy or occipital SFAR-PSD as the

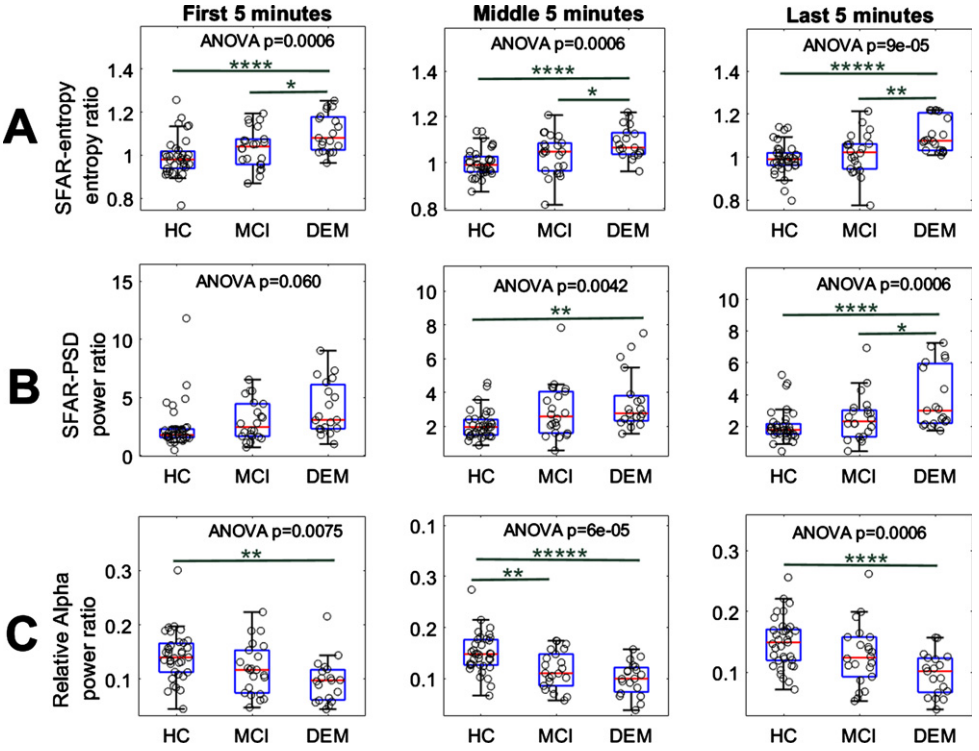

Fig. 3. Assessment of SFAR-entropy and SFAR-PSD measures across REM cycles in the night. All measures were calculated in the occipital region. A) The slow-to-fast activity ratio of MFDE (SFAR-entropy) for the first, middle, and last 5 min of REM sleep, for HC, MCI, and DEM. B) SFAR-PSD for the first, middle, and last 5 min of REM sleep, for HC, MCI, and DEM. C) Relative alpha power for the first, middle, and last 5 min of REM sleep, for HC, MCI, and DEM. The ANOVA omnibus p-value is listed in each boxplot (Bonferroni corrected). The Tukey *post-hoc* comparisons with p-values smaller than 0.05, 0.01, 0.001, 0.0001, and 0.00001 are shown with *, **, ***, ****, and *****, respectively.

Table 2
Coefficient of variation (CV) for SFAR-entropy, SFAR-PSD, and relative alpha power in HC, MCI, and DEM

	SFAR-entropy	SFAR-PSD	Relative alpha power	ANOVA p-value
CV in HC (mean ± SD)	0.06 ± 0.02	0.45 ± 0.40	0.24 ± 0.07	p = 1e-09; entropy vs. PSD, p = 1e-09; entropy vs. alpha, p = 0.0047; PSD vs. alpha, p = 6e-04
CV in MCI (mean ± SD)	0.06 ± 0.03	0.40 ± 0.14	0.26 ± 0.06	p = 2e-18; entropy vs. PSD, p = 1e-10; entropy vs. alpha, p = 2e-09; PSD vs. alpha, p = 4e-06
CV in DEM (mean ± SD)	0.06 ± 0.02	0.32 ± 0.10	0.26 ± 0.07	p = 1e-16; entropy vs. PSD, p = 1e-10; entropy vs. alpha, p = 1e-10; PSD vs. alpha, p = 0.016

SD, standard deviation.

sole input feature. Model performances were compared using cross-validated AUC_{ROC} and AUC_{PR} (Fig. 6). For discriminating DEM versus HC, the SFAR-entropy model had excellent performance based on the AUC_{ROC} (AUC_{ROC} = 0.870 [0.809, 0.925]), and performed significantly better than the SFAR-PSD model (AUC_{ROC} = 0.802 [0.715, 0.883]) (p = 0.037). A similar trend was also seen with the AUC_{PR}, where the SFAR-entropy model had higher performance than the SFAR-PSD model, though this was not statistically significant (0.942 [0.888, 0.992] versus 0.894 [0.809, 0.981], respectively, p = 0.102; AUC_{PR} for chance-level performance = 0.648).

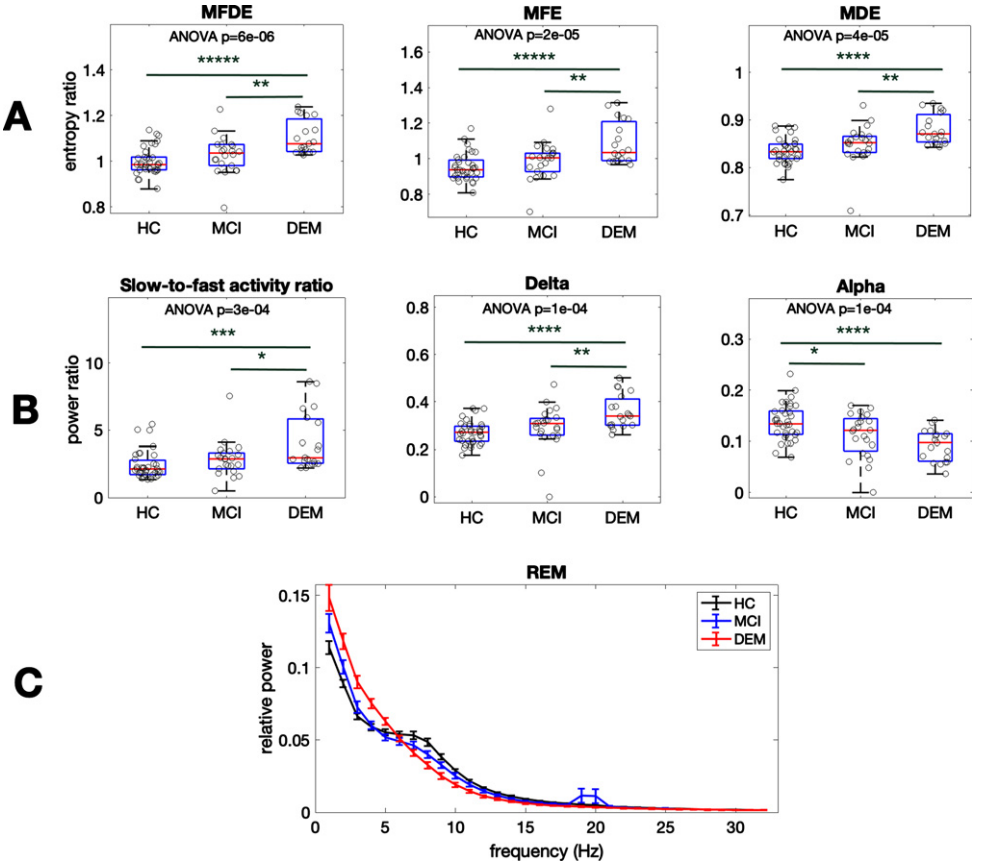

Fig. 4. Comparison of MFDE to additional entropy and spectral measures in REM sleep to discriminate Alzheimer's disease dementia. A) Comparison of slow-to-fast activity ratio of various entropy measures, including MFDE, multiscale fuzzy entropy (MFE), and multiscale dispersion entropy (MDE), to discriminate HC, MCI, and DEM in REM sleep. B) Comparison of spectral measures, including slow-to-fast activity ratio of the PSD (SFAR-PSD), relative delta power, and relative alpha power, to discriminate HC, MCI, and DEM in REM sleep. For (A) and (B), ANOVA p values are listed, and differences with p-values smaller than 0.05, 0.01, 0.001, 0.0001, and 0.00001 are respectively shown with *, **, ***, ****, and *****. C) Relative power spectral density curves for HC (black), MCI (blue), and DEM (red).

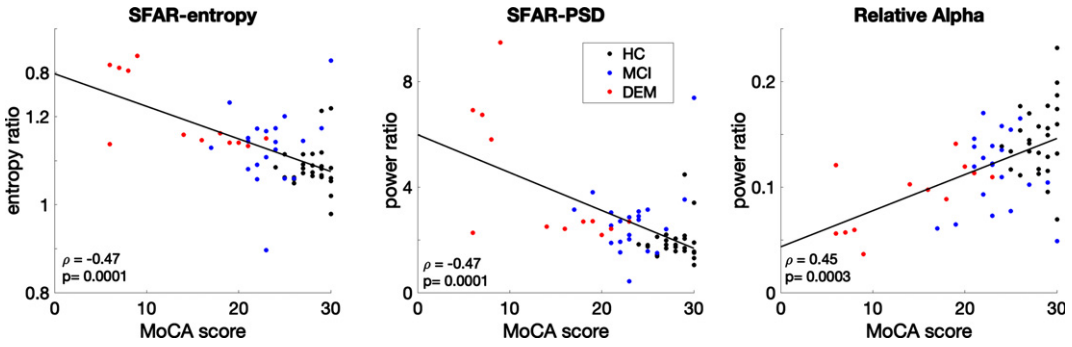

Fig. 5. Correlation of SFAR-entropy, SFAR-PSD, and relative alpha with MoCA scores. SFAR-entropy (left), SFAR-PSD (middle), and relative alpha (right) were calculated from the occipital region during REM sleep. Spearman correlations are shown.

For discriminating DEM versus MCI, the SFAR-entropy model also performed well ($AUC_{ROC} = 0.708$ [0.580, 0.830]), and was significantly better than the SFAR-PSD model ($AUC_{ROC} = 0.590$ [0.414, 0.744]) ($p = 0.010$). This difference was also seen with the AUC_{PR}, where the SFAR-entropy model out-

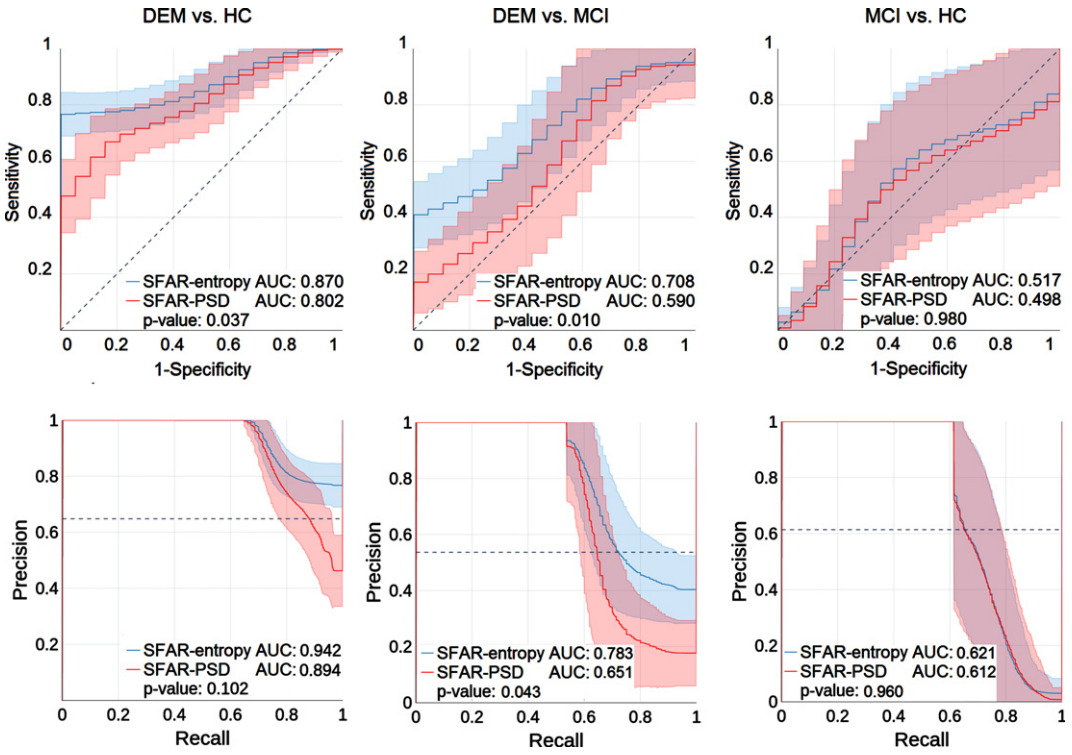

Fig. 6. Classification performance of SFAR-entropy and SFAR-PSD in REM sleep in discriminating HC, MCI, and DEM. ROC (top row) and PR (bottom row) curves for logistic regression classifiers based on SFAR-entropy (blue) and SFAR-PSD (red), for discrimination between DEM versus HC (left), DEM versus MCI (middle), and MCI versus HC (right). Both SFAR-entropy and SFAR-PSD were calculated from the occipital region during REM sleep. Shaded regions represent the 95% confidence intervals for each curve based on bootstrapping. Black dashed lines represent the expected performance for a random classifier.

performed the SFAR-PSD model ($AUC_{PR} = 0.783$ [0.636, 0.943] versus 0.651 [0.456, 0.840], $p = 0.043$; AUC_{PR} for chance-level performance = 0.536).

Both SFAR-entropy and SFAR-PSD performed at only chance-level prediction in discriminating MCI versus HC ($AUC_{ROC} = 0.517$ [0.286, 0.738] and 0.498 [0.247, 0.737], respectively, and $AUC_{PR} = 0.621$ [0.431, 0.805] and 0.612 [0.408, 0.801], respectively, with AUC_{PR} for chance-level performance = 0.614).

Addition of demographic variables (age, sex, and level of education) to the SFAR-entropy and SFAR-PSD models did not significantly improve the performance of either model. The relative alpha power model had similar performance to the SFAR-PSD model (DEM versus HC: $AUC_{ROC} = 0.807$ [0.722 0.887] and $AUC_{PR} = 0.892$ [0.811, 0.977]; DEM versus MCI: $AUC_{ROC} = 0.566$ [0.359 0.771] and $AUC_{PR} = 0.664$ [0.441, 0.886], MCI versus HC: $AUC_{ROC} = 0.597$ [0.463 0.722] and $AUC_{PR} = 0.692$ [0.538, 0.844]).

Test-retest reliability

To assess the night-to-night test-retest reliability of SFAR-entropy, SFAR-PSD, and relative alpha power, we measured the Spearman correlation coefficient (SCC) for 15 participants (7 HC, 5 MCI, and 3 DEM) who each had two consecutive nights of EEG recording. The SFAR-entropy, SFAR-PSD, and relative alpha values at night 2 versus their corresponding values at night 1 are shown in Supplementary Figure 3. The SCC values for SFAR-entropy, SFAR-PSD, and relative alpha power, respectively, were 0.93, 0.81, and 0.96. These results suggest that all three measures have excellent night-to-night reliability.

DISCUSSION

In this study, we compared MFDE, a non-linear measure of information content, on ambulatory scalp EEGs of DEM, MCI, and HC individuals, across awake and sleep states. We found that the

slow-to-fast-activity MFDE ratio (SFAR-entropy) differentiated DEM from both MCI and HC in REM sleep. Just 5 min of REM sleep was sufficient for SFAR-entropy to discriminate DEM from HC and MCI, and this discriminatory power remained stable across REM cycles throughout the night. Consistent with prior work [47], SFAR-PSD during REM sleep showed a similar capacity to distinguish DEM from HC and MCI. Even so, the coefficient of variation for SFAR-entropy in REM sleep was significantly lower than for SFAR-PSD and relative alpha power, and SFAR-entropy had a greater effect size for the discrimination of DEM from HC. Increases in both SFAR-entropy and SFAR-PSD and decreases in relative alpha power during REM sleep were associated with worse performance on the MoCA. However, logistic regression classifiers that used SFAR-entropy as an input feature showed significantly better performance in distinguishing DEM versus HC, and DEM versus MCI, compared to classifiers that used SFAR-PSD. Thus, while our results complement previous reports showing that changes in slow-to-fast activity ratio in REM sleep based on PSD (SFAR-PSD) can discriminate DEM from MCI and HC [32, 47, 59], SFAR-entropy outperformed SFAR-PSD on both diagnostic classification accuracy and the extent of its variability.

Although impairments of NREM sleep in AD are well-described [19–25], AD-associated changes of REM sleep have received little attention. Given that basal forebrain cholinergic neurons that project diffusely to cortex are particularly active in REM sleep [29–31] and degenerate in AD [26–28], the fact that discrimination between DEM and HC is greatest in REM sleep is not unexpected. While basal forebrain cholinergic neurons are active in the awake state, the rsEEG is also impacted by the activity of other neuromodulatory systems such as the ascending noradrenergic system that contributes to arousal and attention. Thus, the EEG in REM sleep may be particularly well-suited to detect and study repercussions of basal forebrain cholinergic dysfunction. Furthermore, as recent work has demonstrated a causal role for REM sleep in learning and memory [60], the AD-associated REM sleep SFAR-entropy deficits shown here may bear directly on the neural systems failure that contributes to dementia in AD.

In this study, 68% of DEM participants were taking acetylcholinesterase inhibitors at the time of their EEG, compared to only 39% of MCI, and none of the HC. Prior work in patients with mild to moderate dementia due to AD showed that chronic treatment with the acetylcholinesterase inhibitor, donepezil, reduced delta and theta power and reduced SFAR-PSD during REM sleep [61], effects which would serve to diminish the difference in SFAR-entropy between diagnostic groups. Thus, the "biological" difference in SFAR-entropy between DEM and the MCI and HC groups during REM sleep may be even greater than that observed here. In any case, SFAR entropy continued to differentiate DEM from MCI and HC groups when the analyses were restricted to participants who were not taking acetylcholinesterase inhibitors. Interestingly, we found no consistent differences between MCI and HC for SFAR-entropy or SFAR-PSD across REM sleep or any sleep state. While the basis for this observation is unclear, it is worth noting that the differential use of acetylcholinesterase inhibitors across MCI and HC groups may have reduced the sensitivity of these measures to differentiate these groups. In addition, as amyloid burden in cognitively normal older people has been associated with cortical synaptic cholinergic deficits that may impact the EEG measures evaluated here [62, 63], cortical amyloid among HC participants, if present, may have reduced differences between MCI and HC. Future studies that account for amyloid burden and the integrity of the basal forebrain cholinergic system will be informative.

While we used MFDE as our primary entropy measure, we found that other entropy measures, including MFE and MDE, performed similarly. Thus, the reduction of entropy during REM sleep that we observed in AD appears to be a robust phenomenon. From the standpoint of computational cost and ease of calculation, MFDE is superior to MFE and MDE [37, 38].

Strengths of this study include the evaluation of well-characterized clinical populations of both DEM and MCI. Participants were well-matched for age and other demographic features. The evaluation of sleep and wake EEG permitted detailed quantitative measurements across behavioral states that have been less well studied to date than conventional rsEEG. In addition, to our knowledge, this is the first evaluation in AD of nonlinear EEG measures across a range of biologically relevant time-scales, including MFDE and its contrast with the SFAR-PSD, during sleep. There were also a number of limitations. One limitation is the use of clinically diagnosed groups, without biomarker or neuropathologic confirmation. Even so, patients were recruited from a tertiary care center dementia facility and carefully reviewed by two dementia specialists for inclusion in the study.

Another limitation is the lack of sufficient data in the NREM3 sleep state to permit its evaluation in the current study. Although our sample sizes were modest, potentially reducing the power to detect subtle effects, the primary findings that demonstrated discrimination of DEM from HC and MCI were robust. Future work investigating the functional connectivity and high-order interactions of sleep EEG brain networks with nonlinear methods in MCI and dementia will be informative [64].

Together, the present findings support further study of the EEG-based SFAR-entropy measure in REM sleep, both as a diagnostic biomarker for early stages of AD and as a physiologic measure reflecting neural systems integrity that may be prove useful in AD clinical trials.

ACKNOWLEDGMENTS

The authors thank all individuals who participated in this study; and Kyle Pellerin for technical assistance.

FUNDING

The work was supported by NIH P30AG062421 (SNG) and NIH K23NS101037 (ADL).

CONFLICT OF INTEREST

The authors have no relevant conflicts of interest to report. Sebastian Moguilner has received research funding from the Alzheimer's Association. Rani Sarkis received grants from the National Institutes of Health (K23 NS119798) during the submitted work, and research support from Biogen. Stephen Gomperts has served on Advisory Boards of Jannsen, Acadia, Sanofi, and EIP, has received consulting fees from EIP Pharma, and receives funding from the NIH (R01AG077611, R01AG054551, R01AG066171, 1R56AG070827, U01NS119562, R41NS122576, P30AG062421), the DOD CDMRP, the Michael J. Fox Foundation, the FFFPRI, and the Lewy Body Dementia Association. Alice Lam has received consulting fees from Sage Therapeutics, Neurona Therapeutics, and Cognito Therapeutics, and has received research funding from the NIH (K23NS101037, R21AG064413), the Alzheimer's Association, and Sage Therapeutics.

DATA AVAILABILITY

The data supporting the findings of this study are available on request from the corresponding author.

SUPPLEMENTARY MATERIAL

The supplementary material is available in the electronic version of this article: https://dx.doi.org/10.3233/JAD-221152.

REFERENCES

[1] Alzheimer's Association (2019) 2019 Alzheimer's disease facts and figures. *Alzheimers Dement* **15**, 321-387.

[2] Scheltens P, Blennow K, Breteler MMB, de Strooper B, Frisoni GB, Salloway S, Van der Flier WM (2016) Alzheimer's disease. *Lancet* **388**, 505-517.

[3] Masters CL, Bateman R, Blennow K, Rowe CC, Sperling RA, Cummings JL (2015) Alzheimer's disease. *Nat Rev Dis Primers* **1**, 15056.

[4] Tan CC, Yu JT, Tan L (2014) Biomarkers for preclinical Alzheimer's disease. *J Alzheimers Dis* **42**, 1051-1069.

[5] Hansson O (2021) Biomarkers for neurodegenerative diseases. *Nat Med* **27**, 954-963.

[6] Colom-Cadena M, Spires-Jones T, Zetterberg H, Blennow K, Caggiano A, Dekosky ST, Fillit H, Harrison JE, Schneider LS, Scheltens P, De Haan W, Grundman M, Van Dyck CH, Izzo NJ, Catalano SM (2020) The clinical promise of biomarkers of synapse damage or loss in Alzheimer's disease. *Alzheimers Res Ther* **12**, 21.

[7] Rossini PM, Di Iorio R, Vecchio F, Anfossi M, Babiloni C, Bozzali M, Bruni AC, Cappa SF, Escudero J, Fraga FJ, Giannakopoulos P, Guntekin B, Logroscino G, Marra C, Miraglia F, Panza F, Tecchio F, Pascual-Leone A, Dubois B (2020) Early diagnosis of Alzheimer's disease: The role of biomarkers including advanced EEG signal analysis. Report from the IFCN-sponsored panel of experts. *Clin Neurophysiol* **131**, 1287-1310.

[8] Selkoe DJ (2002) Alzheimer's disease is a synaptic failure. *Science* **298**, 789-791.

[9] Cassani R, Estarellas M, San-Martin R, Fraga FJ, Falk TH (2018) Systematic review on resting-state EEG for Alzheimer's disease diagnosis and progression assessment. *Dis Markers* **2018**, 5174815.

[10] Smailovic U, Jelic V (2019) Neurophysiological markers of Alzheimer's disease: Quantitative EEG approach. *Neurol Ther* **8**, S37-S55.

[11] Babiloni C, Arakaki X, Azami H, Bennys K, Blinowska K, Bonanni L, Bujan A, Carrillo MC, Cichocki A, de Frutos-Lucas J, Del Percio C, Dubois B, Edelmayer R, Egan G, Epelbaum S, Escudero J, Evans A, Farina F, Fargo K, Fernández A, Ferri R, Frisoni G, Hampel H, Harrington MG, Jelic V, Jeong J, Jiang Y, Kaminski M, Kavcic V, Kilborn K, Kumar S, Lam A, Lim L, Lizio R, Lopez D, Lopez S, Lucey B, Maestú F, McGeown WJ, McKeith I, Moretti DV, Nobili F, Noce G, Olichney J, Onofrj M, Osorio R, Parra-Rodriguez M, Rajji T, Ritter P, Soricelli A, Stocchi F, Tarnanas I, Taylor JP, Teipel S, Tucci F, Valdes-Sosa M, Valdes-Sosa P, Weiergräber M, Yener G, Guntekin B (2021) Measures of resting state EEG rhythms for clinical trials in Alzheimer's disease: Rec-

ommendations of an expert panel. *Alzheimers Dement* **17**, 1528-1553.

[12] Meghdadi AH, Stevanović Karić M, McConnell M, Rupp G, Richard C, Hamilton J, Salat D, Berka C (2021) Resting state EEG biomarkers of cognitive decline associated with Alzheimer's disease and mild cognitive impairment. *PLoS One* **16**, e0244180.

[13] King JR, Sitt JD, Faugeras F, Rohaut B, El Karoui I, Cohen L, Naccache L, Dehaene S (2013) Information sharing in the brain indexes consciousness in noncommunicative patients. *Curr Biol* **23**, 1914-1919.

[14] Musaeus CS, Engedal K, Høgh P, Jelic V, Mørup M, Naik M, Oeksengaard AR, Snaedal J, Wahlund LO, Waldemar G (2018) EEG theta power is an early marker of cognitive decline in dementia due to Alzheimer's disease. *J Alzheimers Dis* **64**, 1359-1371.

[15] Babiloni C, Blinowska K, Bonanni L, Cichocki A, De Haan W, Del Percio C, Dubois B, Escudero J, Fernández A, Frisoni G, Guntekin B, Hajos M, Hampel H, Ifeachor E, Kilborn K, Kumar S, Johnsen K, Johannsson M, Jeong J, LeBeau F, Lizio R, Lopes da Silva F, Maestú F, McGeown WJ, McKeith I, Moretti DV, Nobili F, Olichney J, Onofrj M, Palop JJ, Rowan M, Stocchi F, Struzik ZM, Tanila H, Teipel S, Taylor JP, Weiergräber M, Yener G, Young-Pearse T, Drinkenburg WH, Randall F (2020) What electrophysiology tells us about Alzheimer's disease: A window into the synchronization and connectivity of brain neurons. *Neurobiol Aging* **85**, 58-73.

[16] Jelic V, Kowalski J (2009) Evidence-based evaluation of diagnostic accuracy of resting EEG in dementia and mild cognitive impairment. *Clin EEG Neurosci* **40**, 129-142.

[17] Fifel K, Videnovic A (2021) Circadian and sleep dysfunctions in neurodegenerative disorders—an update. *Front Neurosci* **14**, 627330.

[18] Kent BA, Feldman HH, Nygaard HB (2021) Sleep and its regulation: An emerging pathogenic and treatment frontier in Alzheimer's disease. *Prog Neurobiol* **197**, 101902.

[19] Mander BA (2020) Local sleep and Alzheimer's disease pathophysiology. *Front Neurosci* **14**, 525970.

[20] Mander BA, Marks SM, Vogel JW, Rao V, Lu B, Saletin JM, Ancoli-Israel S, Jagust WJ, Walker MP (2015) β-amyloid disrupts human NREM slow waves and related hippocampus-dependent memory consolidation. *Nat Neurosci* **18**, 1051-1057.

[21] Winer JR, Mander BA, Helfrich RF, Maass A, Harrison TM, Baker SL, Knight RT, Jagust WJ, Walker MP (2019) Sleep as a potential biomarker of Tau and β-amyloid burden in the human brain. *J Neurosci* **39**, 6315-6324.

[22] Lucey BP, McCullough A, Landsness EC, Toedebusch CD, McLeland JS, Zaza AM, Fagan AM, McCue L, Xiong C, Morris JC, Benzinger TLS, Holtzman DM (2019) Reduced non–rapid eye movement sleep is associated with tau pathology in early Alzheimer's disease. *Sci Transl Med* **11**, eaau6550.

[23] Ju YS, Ooms SJ, Sutphen C, Macauley SL, Zangrilli MA, Jerome G, Fagan AM, Mignot E, Zempel JM, Claassen JAHR, Holtzman DM (2017) Slow wave sleep disruption increases cerebrospinal fluid amyloid-b levels. *Brain* **140**, 2104-2111.

[24] Helfrich RF, Mander BA, Jagust WJ, Knight RT, Walker MP (2017) Old brains come uncoupled in sleep: Slow wave-spindle synchrony, brain atrophy, and forgetting. *Neuron* **97**, 221-230.e4.

[25] De Gennaro L, Gorgoni M, Reda F, Lauri G, Truglia I, Cordone S, Scarpelli S, Mangiaruga A, D'Atri A, Lacidogna G, Ferrara M, Marra C, Rossini PM (2017) The fall of sleep K-complex in Alzheimer disease. *Sci Rep* **7**, 39688.

[26] Bowen DM, Benton JS, Spillane JA, Smith CCT, Allen SJ (1982) Choline acetyltransferase activity and histopathology of frontal neocortex from biopsies of demented patients. *J Neurol Sci* **57**, 191-202.

[27] Whitehouse PJ, Struble RG, Clark AW, Price DL (1982) Alzheimer disease: Plaques, tangles, and the basal forebrain. *Ann Neurol* **12**, 494.

[28] Mufson EJ, Counts SE, Perez SE, Ginsberg SD (2008) Cholinergic system during the progression of Alzheimer's disease: Therapeutic implications. *Expert Rev Neurother* **8**, 1703-1718.

[29] Kodama T, Takahashi Y, Honda Y (1990) Enhancement of acetylcholine release during paradoxical sleep in the dorsal tegmental field of the cat brain stem. *Neurosci Lett* **114**, 277-282.

[30] Vazquez J, Baghdoyan HA (2001) Basal forebrain acetylcholine release during REM sleep is significantly greater than during waking. *Am J Physiol Integr Comp Physiol* **280**, R598-R601.

[31] Kametani H, Kawamura H (1990) Alterations in acetylcholine release in the rat hippocampus during sleep-wakefulness detected by intracerebral dialysis. *Life Sci* **47**, 421-426.

[32] Petit D, Montplaisir J, Lorrain D, Gauthier S (1992) Spectral analysis of the rapid eye movement sleep electroencephalogram in right and left temporal regions: A biological marker of Alzheimer's disease. *Ann Neurol* **32**, 172-176.

[33] Breakspear M (2017) Dynamic models of large-scale brain activity. *Nat Neurosci* **20**, 340-352.

[34] Hornero R, Abásolo D, Escudero J, Gómez C (2009) Nonlinear analysis of electroencephalogram and magnetoencephalogram recordings in patients with Alzheimer's disease. *Philos Trans A Math Phys Eng Sci* **367**, 317-336.

[35] Dauwels J, Vialatte F, Cichocki A (2010) Diagnosis of Alzheimer's disease from EEG signals: Where are we standing? *Curr Alzheimer Res* **7**, 487-505.

[36] Costa M, Goldberger AL, Peng CK (2005) Multiscale entropy analysis of biological signals. *Phys Rev E Stat Nonlin Soft Matter Phys* **71**, 021906.

[37] Azami H, Rostaghi M, Abasolo D, Escudero J (2017) Refined composite multiscale dispersion entropy and its application to biomedical signals. *IEEE Trans Biomed Eng* **64**, 2872-2879.

[38] Azami H, Arnold SE, Sanei S, Chang Z, Sapiro G, Escudero J, Gupta AS (2019) Multiscale fluctuation-based dispersion entropy and its applications to neurological diseases. *IEEE Access* **7**, 68718-68733.

[39] Lam AD, Sarkis RA, Pellerin KR, Jing J, Dworetzky BA, Hoch DB, Jacobs CS, Lee JW, Weisholtz DS, Zepeda R, Westover MB, Cole AJ, Cash SS (2020) Association of epileptiform abnormalities and seizures in Alzheimer disease. *Neurology* **95**, e2259-e2270.

[40] Abou Jaoude M, Sun H, Pellerin KR, Pavlova M, Sarkis RA, Cash SS, Westover MB, Lam AD (2020) Expert-level automated sleep staging of long-term scalp electroencephalography recordings using deep learning. *Sleep* **43**, zsaa112.

[41] Albert MS, DeKosky ST, Dickson D, Dubois B, Feldman HH, Fox NC, Gamst A, Holtzman DM, Jagust WJ, Petersen RC, Snyder PJ, Carrillo MC, Thies B, Phelps CH (2011) The diagnosis of mild cognitive impairment due to Alzheimer's disease: Recommendations from the National Institute on Aging-Alzheimer's Association workgroups on diagnostic

guidelines for Alzheimer's disease. *Alzheimers Dement* **7**, 270-279.

[42] McKhann GM, Knopman DS, Chertkow H, Hyman BT, Jack CR Jr, Kawas CH, Klunk WE, Koroshetz WJ, Manly JJ, Mayeux R, Mohs RC, Morris JC, Rossor MN, Scheltens P, Carrillo MC, Thies B, Weintraub S, Phelps CH (2011) The diagnosis of dementia due to Alzheimer's disease: Recommendations from the National Institute on Aging-Alzheimer's Association workgroups on diagnostic guidelines for Alzheimer's disease. *Alzheimers Dement* **7**, 263-269.

[43] McKeith I, Boeve BF, Dickson DW, Halliday G, Taylor JP, Weintraub D, Aarsland D, Galvin J, Attems J, Ballard CG, Bayston A, Beach TG, Blanc F, Bohnen N, Bonanni L, Bras J, Brundin P, Burn D, Chen-Plotkin A, Duda JE, El-Agnaf O, Feldman H, Ferman TJ, Ffytche D, Fujishiro H, Galasko D, Goldman JG, Gomperts SN, Graff-Radford NR, Honig LS, Iranzo A, Aarsland D, Attems J, Ballard CG, Bayston A, Beach TG, Chen-plotkin A, Singleton A, Taylor A (2017) Diagnosis and management of dementia with Lewy bodies: Fourth consensus report of the DLB Consortium. *Neurology* **89**, 88-100.

[44] Rascovsky K, Hodges JR, Knopman D, Mendez MF, Kramer JH, Neuhaus J, Van Swieten JC, Seelaar H, Dopper EGP, Onyike CU, Hillis AE, Josephs KA, Boeve BF, Kertesz A, Seeley WW, Rankin KP, Johnson JK, Gorno-Tempini ML, Rosen H, Prioleau-Latham CE, Lee A, Kipps CM, Lillo P, Piguet O, Rohrer JD, Rossor MN, Warren JD, Fox NC, Galasko D, Salmon DP, Black SE, Mesulam M, Weintraub S, Dickerson BC, Diehl-Schmid J, Pasquier F, Deramecourt V, Lebert F, Pijnenburg Y, Chow TW, Manes F, Grafman J, Cappa SF, Freedman M, Grossman M, Miller BL (2011) Sensitivity of revised diagnostic criteria for the behavioural variant of frontotemporal dementia. *Brain* **134**, 2456-2477.

[45] Sachdev P, Kalaria R, O'Brien J, Skoog I, Alladi S, Black SE, Blacker D, Blazer DG, Chen C, Chui H, Ganguli M, Jellinger K, Jeste D V., Pasquier F, Paulsen J, Prins N, Rockwood K, Roman G, Scheltens P (2014) Diagnostic criteria for vascular cognitive disorders: A VASCOG statement. *Alzheimer Dis Assoc Disord* **28**, 206-218.

[46] Roalf DR, Moberg PJ, Xie SX, Wolk DA, Moelter ST, Arnold SE (2013) Comparative accuracies of two common screening instruments for classification of Alzheimer's disease, mild cognitive impairment, and healthy aging. *Alzheimers Dement* **9**, 529-537.

[47] Brayet P, Petit D, Frauscher B, Gagnon JF, Gosselin N, Gagnon K, Rouleau I, Montplaisir J (2016) Quantitative EEG of rapid-eye-movement sleep: A marker of amnestic mild cognitive impairment. *Clin EEG Neurosci* **47**, 134-141.

[48] Rostaghi M, Azami H (2016) Dispersion entropy: A measure for time-series analysis. *IEEE Signal Process Lett* **23**, 610-614.

[49] Azami H, Escudero J (2018) Amplitude- and fluctuation-based dispersion entropy. *Entropy (Basel)* **20**, 210.

[50] Miskovic V, MacDonald KJ, Rhodes LJ, Cote KA (2019) Changes in EEG multiscale entropy and power-law frequency scaling during the human sleep cycle. *Hum Brain Mapp* **40**, 538-551.

[51] Sukriti, Chakraborty M, Mitra D (2021) Automated detection of epileptic seizures using multiscale and refined composite multiscale dispersion entropy. *Chaos Solitons Fractals* **146**, 110939.

[52] Kafantaris E, Piper I, Lo TM, Escudero J (2020) Augmentation of dispersion entropy for handling missing and outlier samples in physiological signal monitoring. *Entropy (Basel)* **22**, 319.

[53] Tripathy RK, Acharya UR (2018) Use of features from RR-time series and EEG signals for automated classification of sleep stages in deep neural network framework. *Biocybern Biomed Eng* **38**, 890-902.

[54] Zhao L, Wei S, Tang H, Liu C (2016) Multivariable fuzzy measure entropy analysis for heart rate variability and heart sound amplitude variability. *Entropy (Basel)* **18**, 430.

[55] Azami H, Escudero J (2018) Coarse-graining approaches in univariate multiscale sample and dispersion entropy. *Entropy (Basel)* **20**, 138.

[56] Azami H, Fernández A, Escudero J (2017) Refined multiscale fuzzy entropy based on standard deviation for biomedical signal analysis. *Med Biol Eng Comput* **55**, 2037-2052.

[57] Abraham A, Pedregosa F, Eickenberg M, Gervais P, Mueller A, Kossaifi J, Gramfort A, Thirion B, Varoquaux G (2014) Machine learning for neuroimaging with scikit-learn. *Front Neuroinform* **8**, 14.

[58] Altman DG, Bland JM (2011) How to obtain the P value from a confidence interval. *BMJ* **343**, d2304.

[59] Petit D, Lorrain D, Gauthier S, Montplaisir J (1993) Regional spectral analysis of the REM sleep EEG in mild to moderate Alzheimer's disease. *Neurobiol Aging* **14**, 141-145.

[60] Boyce R, Glasgow SD, Williams S, Adamantidis A (2016) Causal evidence for the role of REM sleep theta rhythm in contextual memory consolidation. *Science* **352**, 812-816.

[61] dos Santos Moraes WA, Poyares DR, Guilleminault C, Ramos LR, Bertolucci PHF, Tufik S (2006) The effect of donepezil on sleep and REM sleep EEG in patients with Alzheimer disease: A double-blind placebo-controlled study. *Sleep* **29**, 199-205.

[62] Potter PE, Rauschkolb PK, Pandya Y, Sue LI, Sabbagh MN, Walker DG, Beach TG (2011) Pre-and post-synaptic cortical cholinergic deficits are proportional to amyloid plaque presence and density at preclinical stages of Alzheimer's disease. *Acta Neuropathol* **122**, 49-60.

[63] Beach TG, Kuo Y-M, Spiegel K, Emmerling MR, Sue LI, Kokjohn K, Roher AE (2000) The cholinergic deficit coincides with Aβ deposition at the earliest histopathologic stages of Alzheimer disease. *J Neuropathol Exp Neurol* **59**, 308-313.

[64] Herzog R, Rosas FE, Whelan R, Fittipaldi S, Santamaria-Garcia H, Cruzat J, Birba A, Moguilner S, Tagliazucchi E, Prado P (2022) Genuine high-order interactions in brain networks and neurodegeneration. *Neurobiol Dis* **175**, 105918.